

Effects of broken time-reversal symmetry on transmission zeros

Tae-Suk Kim

Institute of Physics and Applied Physics, Yonsei University, Seoul 120-749, Korea

Sam Young Cho and Chul Koo Kim

Institute of Physics and Applied Physics, Yonsei University, Seoul 120-749, Korea

*Center for Strongly Correlated Materials Research,
Seoul National University, Seoul 151-742, Korea*

Chang-Mo Ryu

Department of Physics, Pohang University of Science and Technology, Pohang 790-784, Korea

(Dated: May 21, 2019)

In this paper, we study the behavior of the transmission zeros and the corresponding change in the transmission phase when the time-reversal symmetry is broken by magnetic fields. For our study, we consider the closed Aharonov-Bohm(AB) interferometer with various embedded scattering centers. We find the following: (i) The transmission zeros are real when the AB flux is an integer or a half-integer multiple of the flux quantum, and the transmission phase jumps by π at the zeros. (ii) The transmission zeros become complex or are shifted off the real-energy axis when the magnetic AB flux is not an integer or a half-integer multiple of the flux quantum, and the transmission phase evolves continuously. (iii) The distance of the zeros from the real-energy axis or the imaginary part of the transmission zeros is sinusoidal as a function of the magnetic AB phase. We suggest the experimental setup which can test our results.

PACS numbers: 73.23.-b, 73.50.Bk, 73.63.Nm

I. INTRODUCTION

Recently advanced nanotechnology has made it possible to measure the phase of electron wave functions^{1,2,3,4,5}. In bulk systems, the electron's phase can be washed out by several inelastic scattering processes. On the other hand, the phase of the electron wave function can be preserved in nanoscopic systems. Typical experimental tools, which can measure the electron's phase, are the Aharonov-Bohm (AB) interferometers. To study the phase evolution of the interesting target system, the target system is inserted in one of two arms of the AB interferometer. The I-V curves are measured between the external electrodes connected to the AB ring as a function of the AB magnetic flux while other control parameters, e.g., the Fermi energy level, are varied. The phase of the electron wave functions in the target system is extracted from the measured I-V curves.

The closed AB interferometer in a two-terminal configuration cannot give much information about the phase of the target system due to the Onsager relation. Multiple windings of electron's motion along the AB ring result in the conductance which is even in the AB flux⁶ or $G(-B) = G(B)$. The Onsager relation constrains that the measured conductance be a local maximum or a local minimum at, say, $B = 0$. The transition from maximum (minimum) to minimum (maximum) occurs sharply both at the transmission peak¹ (the real part of the transmission pole changes its sign) and somewhere between two neighboring transmission peaks. The measured phase can be either 0 or π . But this phase is *not* the phase of the target system.

To see the phase evolution of the target system, the open AB interferometer is devised by Schuster, et. al.², which is similar to the double-slit experiments. Suppression of the back-scattered electrons prevents the multiple scattering processes so that the total transmission amplitude is the sum of two transmission amplitudes through the upper and lower arms,

$$t = t_l + t_u e^{i\phi}. \quad (1)$$

Here ϕ is the AB phase due to the magnetic flux. Measuring the conductance which is proportional to $|t|^2$ as a function of the AB phase, the transmission phase of the target system can be directly obtained.

In the phase-coherent systems, the two different phases can be defined. The Friedel phase θ_f is defined as the argument of the determinant of the scattering S -matrix, $e^{2i\theta_f} = \det S$. The change in the Friedel phase is related to the density of states via the Friedel sum rule⁷, $\rho(E) = \pi^{-1} d\theta_f / dE$. The measured phase in the open AB interferometers is in fact the transmission phase, the argument of the transmission amplitudes ($t = |t|e^{i\theta_t}$). Recent works^{8,9} made clear distinctions between the two phases. In the absence of the transmission zeros, the two phases are identical. The transmission phase jumps by π at the real transmission zeros and the two phases differ by this amount⁹. In the time-reversal symmetric systems, all the possible transmission zeros are proven to be *real*^{8,10}. For more details about the transmission phase in the time-reversal symmetric case, see the works of Lee⁸ and of Taniguchi and Büttiker⁹.

We may ask what will happen to the transmission zeros and the transmission phase when the time-reversal sym-

metry is broken by the external fields, e.g., the magnetic fields. In this paper, we want to answer this question by studying the closed AB ring (see Fig. 1) with an embedded scattering center in the presence of the magnetic AB flux. Since the AB ring provides the transmission zeros due to the destructive interference between two arms and the time-reversal symmetry can be broken by applying the magnetic fields, the AB interferometer is an ideal system for our purpose.

In general, either one transmission pole or one transmission zero gives rise to the phase change by π as the Fermi energy is scanned through the real part of pole or zero. The poles always lie in the lower half-plane of the complex-energy plane due to the causality relation, but the zeros can be anywhere in the complex-energy plane. Poles give the same contribution to the Friedel phase θ_f and the transmission phase θ_t . The energy scale over which the phase evolution occurs is set by the imaginary part of the transmission poles. On the other hand, transmission zeros give an additional contribution θ_z only to the transmission phase. The transmission phase can be written as the sum of two: $\theta_t = \theta_f + \theta_z$. Depending on the position of zeros in the complex-energy plane, the behavior of the phase evolution is quite different. When the transmission zeros lie on the real-energy axis, the abrupt phase jump by π is observed. Varying the AB magnetic flux, the transmission zeros can be shifted off the real-energy axis. In this case, the transmission phase evolution is continuous and occurs over the energy scale – the imaginary part of transmission zeros – as the Fermi energy is scanned. That is, the transmission phase becomes a discontinuous function of control parameters when the transmission zeros hit the real-energy axis.

To summarize the results of our study, the transmission zeros of t (the transmission amplitude of the closed AB ring), based on their position in the complex-energy plane, can be grouped into three different classes.

- Class I: Transmission zeros lie on the real-energy axis. The trajectory of the transmission amplitude t passes through the origin and the transmission phase θ_t jumps by π at the transmission zero.
- Class II: Poles and zeros lie in the same lower half-plane of the 2d complex-energy plane. The trajectory does not encircle the origin and the evolution of θ_t is continuous and its range is confined by two extreme points of the trajectory when viewed from the origin. Each pole and zero give rise to the phase change by π , but the sign is opposite. The combined effect of one pole and one zero is a smooth evolution of θ_t and the difference $\Delta\theta_t$ before and after passing through one zero and one pole approaches 0 or $\Delta\theta_t = 0$.
- Class III: Poles(zeros) lie in the lower(upper) half-plane, respectively. The trajectory encircles the origin. One pole and one zero give the same sign of the phase evolution and $\Delta\theta_t = 2\pi$.

Depending on the nature of the scattering centers which are inserted into one arm of the AB interferometer, all three classes or some of them can be realized with varying magnetic AB flux. We find from our study that the transmission zeros are real when the AB flux is an integer or a half-integer multiple of the flux quantum, and the transmission phase jumps by π at the zeros. The transmission zeros become complex or are shifted off the real-energy axis when the magnetic AB flux is not an integer or a half-integer multiple of the flux quantum, and the transmission phase evolves continuously. The distance of the zeros from the real-energy axis or the imaginary part of the transmission zeros are sinusoidal as a function of the magnetic AB phase.

The general formulation of the S -matrix for the AB ring is presented in the Appendix A when some scattering centers are present along the arms of the AB ring. These scattering centers and the accrued phase by the motion along the AB ring can be parameterized by the matrices \mathcal{R} 's and \mathcal{T} 's as described in the Appendix A. In this paper, we are interested in the AB ring (see Fig. 1) when the interesting target system is inserted in the lower arm. When the target system is described by the scattering matrix $S_0 = \begin{pmatrix} r_0 & t_0 \\ t_0 & r_0' \end{pmatrix}$, the matrices \mathcal{R} 's and \mathcal{T} 's are given by the generic form,

$$\begin{aligned} \mathcal{R} &= z_F \begin{pmatrix} 0 & 0 \\ 0 & r_0 \end{pmatrix}, \quad \mathcal{T} = z_F \begin{pmatrix} e^{i\phi/2} & 0 \\ 0 & t_0 e^{-i\phi/2} \end{pmatrix}, \\ \mathcal{R}' &= z_F \begin{pmatrix} 0 & 0 \\ t_0 & r_0' \end{pmatrix}, \quad \mathcal{T}' = z_F \begin{pmatrix} e^{-i\phi/2} & 0 \\ 0 & t_0' e^{i\phi/2} \end{pmatrix}. \end{aligned} \quad (2)$$

Here $\phi = 2\pi\Phi \cdot e/hc$ is the AB phase due to the magnetic flux Φ passing through the AB ring. The half of the AB phase is attached to each of the lower and upper arms of the AB ring. The trajectory of t depends on the chosen gauge or how the AB phase is inserted into the scattering matrix. Of course, the measurable quantities like $|t|^2$ and $\Delta\theta_t$ do not depend on the gauge. $z_F = e^{ik_F L}$ is the phase accrued by the motion of electrons along either of two arms of length L . Since we are interested in the phase-coherent system, we restrict our study to $T = 0$ K. The incident electrons will be confined to the Fermi energy with the wave number k_F in our study.

In subsequent sections, we study the properties of the transmission amplitude when one target system is inserted in one arm of the AB ring. In Sec. II, we consider the AB interferometer with one discrete energy level. This system is simple enough to find the S -matrix in a closed form and allows one to study analytically the behavior of the transmission zero under the AB flux. In Sec. III and IV, we study the AB ring when two different types of multi resonant level systems are inserted in the lower arm. In Sec. III, we study the transmission properties of the AB ring with an embedded double-barrier well. The double-barrier well provides multi discrete energy levels through which the resonant tunneling is realized, but the transmission probability never becomes zero for this system. In Sec. IV, the t -stub with the double-

barrier is inserted in the AB ring. In contrast to the double-barrier well, the t -stub accommodates the transmission zeros as well as the multi resonant levels. Our study is summarized in Sec. V.

II. AB INTERFEROMETER WITH AN EMBEDDED RESONANT LEVEL

In this section, we consider the Aharonov-Bohm interferometer shown in Fig. 2. This model system may be the simplest one which can accommodate the zero-pole pair in the transmission amplitude. This system contains both the direct tunneling between two leads and the resonant tunneling through one discrete energy level in the dot. The study of this simple model system can help us to analyze more realistic and complex systems to be discussed in the subsequent sections. The transmission amplitude of this system is characterized with one pole and one zero. The pole is provided by the discrete level in a dot while the zero is the result of the destructive interference in the AB ring geometry. Three different classes in the trajectories of t , summarized in the introduction, can be all realized with the variation of the AB phase.

We can derive the scattering matrix of the AB interferometer using the t -matrix method with $S_{ij} = \delta_{ij} - 2\pi\delta(E_i - E_j)T_{ij}$ or the Green's function method.

$$S_{\text{ring}} = \begin{pmatrix} r_{LL} & t_{RL} \\ t_{LR} & r_{RR} \end{pmatrix}, \quad (3)$$

where the reflection and transmission amplitudes are given by the equations,

$$t_{RL} = -i\sqrt{T_0} - \bar{\Gamma}G_d^r(\epsilon) \left[\sqrt{T_0} + \sqrt{g} \sin \phi + i\sqrt{g(1-T_0)} \cos \phi \right], \quad (4a)$$

$$t_{LR} = -i\sqrt{T_0} - \bar{\Gamma}G_d^r(\epsilon) \left[\sqrt{T_0} - \sqrt{g} \sin \phi + i\sqrt{g(1-T_0)} \cos \phi \right], \quad (4b)$$

$$r_{LL} = \sqrt{1-T_0} - \bar{\Gamma}G_d^r(\epsilon) \times \left[\frac{2i}{1+\gamma} - 2i\frac{\Gamma_R}{\Gamma} + \sqrt{gT_0} \cos \phi \right], \quad (4c)$$

$$r_{RR} = \sqrt{1-T_0} - \bar{\Gamma}G_d^r(\epsilon) \times \left[\frac{2i}{1+\gamma} - 2i\frac{\Gamma_L}{\Gamma} + \sqrt{gT_0} \cos \phi \right]. \quad (4d)$$

The angle ϕ is the Aharonov-Bohm phase $2\pi\Phi/\Phi_0$, where Φ is the magnetic flux threading through the AB ring and $\Phi_0 = hc/e$ is the flux quantum. The gauge is chosen such that the AB phase ϕ is attached to the tunneling matrix V_{dR} as $V_{dR} = |V_{dR}|e^{i\phi}$. $T_0 = 4\gamma/(1+\gamma)^2$ is the direct tunneling probability, where $\gamma = \pi^2 N_L N_R |T_{LR}|^2$. N_L and N_R are the density of states(DOS) in the left and right leads, respectively. Other parameters are defined as $\Gamma_p = \pi N_p |V_{dp}|^2$ ($p = L, R$), $\Gamma = \Gamma_L + \Gamma_R$, $\bar{\Gamma} = \Gamma/(1+\gamma)$, and $g = 4\Gamma_L \Gamma_R / \Gamma^2$.

The S -matrix satisfies the Onsager relation, $S_{ij}(\phi) = S_{ji}(-\phi)$ under the inversion of the magnetic flux. If the system is mirror-symmetric under the transformation $L \leftrightarrow R$ or the quantum dot is coupled symmetrically to the left and right leads ($\Gamma_L = \Gamma_R$), we obtain the symmetric relation: $r_{LL} = r_{RR}$.

The discrete energy level in a dot is broadened with the linewidth Γ due to the coupling to the left and right leads. The direct tunneling between the two leads further renormalizes the linewidth($\bar{\Gamma}$) and shifts the energy level position. The retarded Green's function G_d^r of a dot is given by the equation,

$$G_d^r(\epsilon) = \frac{1}{\epsilon - \epsilon_d(\phi) + i\bar{\Gamma}}. \quad (5)$$

Here $\epsilon_d(\phi) = \epsilon_d - \bar{\Gamma}\sqrt{g\gamma} \cos \phi$ is the renormalized energy level of a dot. The transmission probability can be readily calculated from $T(\epsilon) = |t_{RL}|^2$,

$$T(\epsilon) = T_0 + 2\bar{\Gamma}\sqrt{gT_0(1-T_0)} \cos \phi \text{Re}G_d^r + \bar{\Gamma}[T_0 - g(1-T_0 \cos^2 \phi)] \text{Im}G_d^r. \quad (6)$$

The transmission probability $T(\epsilon, \phi)$ is an even function of the AB phase ϕ , satisfying the Onsager relation.

We may rewrite the elements of the scattering matrix in other forms,

$$t_{LR} = -iG_d^r(\epsilon) \left[\sqrt{T_0}(\epsilon - \epsilon_d) + \bar{\Gamma}\sqrt{g}e^{i\phi} \right], \quad (7a)$$

$$t_{RL} = -iG_d^r(\epsilon) \left[\sqrt{T_0}(\epsilon - \epsilon_d) + \bar{\Gamma}\sqrt{g}e^{-i\phi} \right], \quad (7b)$$

$$r_{LL} = G_d^r(\epsilon) \left[\sqrt{R_0}(\epsilon - \epsilon_d) - \bar{\Gamma}\sqrt{g\gamma} \cos \phi + i(\bar{\Gamma}_R - \bar{\Gamma}_L) \right], \quad (7c)$$

$$r_{RR} = G_d^r(\epsilon) \left[\sqrt{R_0}(\epsilon - \epsilon_d) - \bar{\Gamma}\sqrt{g\gamma} \cos \phi - i(\bar{\Gamma}_R - \bar{\Gamma}_L) \right]. \quad (7d)$$

Here $R_0 = 1 - T_0$ is the reflection probability of the direct tunneling. Using the above expressions, we can show the unitarity of the S -matrix, $|t_{LR}|^2 + |r_{LL}|^2 = 1$ and $r_{LL}t_{LR}^* + t_{RL}r_{RR}^* = 0$.

The Friedel phase θ_f can be found from the determinant of S which can be written in terms of the Green's function of a dot,

$$\det S = \frac{G_d^r}{G_d^a} = \frac{\epsilon - \epsilon_d(\phi) - i\bar{\Gamma}}{\epsilon - \epsilon_d(\phi) + i\bar{\Gamma}} = e^{2i\theta_f}, \quad (8a)$$

$$\theta_f = \frac{\pi}{2} + \tan^{-1} \frac{\epsilon - \epsilon_d(\phi)}{\bar{\Gamma}}. \quad (8b)$$

$G_d^a = [G_d^r]^*$ is the advanced Green's function of a dot. The Friedel phase changes smoothly from $\theta_f = 0$ to $\theta_f = \pi$ as the energy level of a dot is scanned through the Fermi energy.

The transmission phase θ_t is obtained from $t = t_{RL} = |t_{RL}|e^{i\theta_t}$ and is written as the sum of the Friedel phase

and the contribution from the zero. The Eq. (7b) can be written as

$$t = -i \frac{(\epsilon - \epsilon_d)\sqrt{T_0} + \bar{\Gamma}\sqrt{g}\cos\phi - i\bar{\Gamma}\sqrt{g}\sin\phi}{\epsilon - \epsilon_d + \bar{\Gamma}\sqrt{g}\cos\phi + i\bar{\Gamma}}. \quad (9)$$

The transmission amplitude at the Fermi energy $t(\epsilon = 0)$ is plotted in the 2d complex plane in Fig. 3(a) and 3(d) as an implicit function of ϵ_d with varying the AB phase ϕ . All the trajectories of t are circles. The position of a discrete energy level ϵ_d , which can be shifted with the gate voltage capacitatively coupled to the dot, is varied from the empty state to the filled state. That is, the value of ϵ_d is changed from ∞ to $-\infty$. Writing $Z = \epsilon - \epsilon_d$, we can rewrite $t = t_{RL}$ as

$$t = -i\sqrt{T_0} \frac{Z - Z_z}{Z - Z_p}, \quad (10)$$

in terms of the pole Z_p and the zero Z_z . This zero-pole pair is given by the expressions,

$$Z_p = -\bar{\Gamma}\sqrt{g}\cos\phi - i\bar{\Gamma}, \quad (11a)$$

$$Z_z = -\bar{\Gamma}\sqrt{\frac{g}{T_0}}[\cos\phi - i\sin\phi]. \quad (11b)$$

Note that the imaginary part of the transmission zero is proportional to $\sin\phi$ and vanishes when $\phi = n\pi$ (n is an integer).

When the magnetic AB flux is an integer or a half-integer multiple of the flux quantum, or when $\phi = n\pi$ (n is an integer), the imaginary part of Z_z vanishes and the transmission zero lies on the real-energy axis. The trajectory of t passes through the origin (the class I). The analytic expression of the transmission phase θ_t when $\phi = n\pi$ is given by the equation,

$$\theta_t = \theta_f + \theta_z, \quad (12a)$$

$$\theta_z = \pi - \pi\Theta(\epsilon - \epsilon_d + (-1)^n\bar{\Gamma}\sqrt{g/T_0}). \quad (12b)$$

Here $\Theta(x)$ is the step function. θ_f is the Friedel phase given by the Eq. (8b) and θ_z is the contribution from the transmission zero. Since the transmission zero is real, the transmission phase jumps abruptly by π as shown in Fig. 3(b) and (e). The zero-pole pair leads to the typical Fano resonance and antiresonance structure in the transmission amplitude $T = |t|^2$ and $T = 0$ at the antiresonance. [See Fig. 5(a) and (f).]

When the magnetic AB flux is off an integer or a half-integer multiple of the flux quantum, the imaginary part of the transmission zero is finite and is sinusoidal as a function of the AB phase ϕ [see the Eq. (11b)]. That is, the zero of t is shifted off the real-energy axis. When $0 < \phi < \pi$, the zero Z_z lies in the upper half-plane of the complex-energy plane while the pole Z_p lies in the lower half-plane. The trajectories of t encircle the origin (the class III). The analytic expression of θ_t is

$$\theta_t = \theta_f + \tan^{-1} \frac{\epsilon - \epsilon_d + \bar{\Gamma}\sqrt{g/T_0}\cos\phi}{\bar{\Gamma}\sqrt{g/T_0}\sin\phi}. \quad (13)$$

The second term is the contribution from the zero. Since both the zero and the pole contribute the same sign of the phase by π to θ_t , θ_t evolves smoothly by the amount of 2π as shown in Fig. 3(b). The imaginary part of the zero is proportional to $\sin\phi$ and the zero moves away linearly with the magnetic field B from the real-energy axis close to $\phi = n\pi$. The minimum value of T (deriving from the transmission zero) shows this trend as displayed in Fig. 3(c). As ϕ is increased from 0 to $\pi/2$, the minimum value of T_{\min} is increased and reaches the maximum at $\phi = \pi/2$. With further increase of ϕ from $\pi/2$ to π , T_{\min} is reduced to zero.

When $\pi < \phi < 2\pi$, the pole and the zero lie in the same lower half-plane. The transmission amplitude, belonging to class II, delineates the closed orbit without encircling the origin. The transmission phase θ_t is given by the expression

$$\theta_t = \theta_f + \pi - \tan^{-1} \frac{\epsilon - \epsilon_d + \bar{\Gamma}\sqrt{g/T_0}\cos\phi}{\bar{\Gamma}\sqrt{g/T_0}|\sin\phi|}. \quad (14)$$

Since the pole and zero contribute the opposite sign of the phase by π to θ_t , the phase evolution is limited to the narrow range [see Fig. 3(e)] which is set by the two extreme points in the trajectory of t viewed from the origin.

In summary, we found the three different classes of the transmission zeros. Though the behavior of the phase evolution is different among three classes, the transmission amplitudes remain in phase before and after the Fermi level is scanned through the real part of the transmission pole and zero. The transmission probability satisfies the Onsager relation, $|t_{RL}(-\phi)|^2 = |t_{RL}(\phi)|^2$ [see Fig. 3(c) and 3(f)], even if the trajectories in the complex t plot are different. When the magnetic flux Φ is the integer or a half-integer multiples of the flux quantum, the transmission zero lies on the real-energy axis and the phase evolution of θ_t is featured with the abrupt jump by π at the zero. When the magnetic flux Φ is off the integer or a half-integer multiples of the flux quantum, the transmission zero lies off the real-energy axis and the phase evolution of θ_t becomes continuous over the energy scale $\bar{\Gamma}\sqrt{g}|\sin\phi|$ set by the magnetic fields. Depending on the sign of the imaginary part of the transmission zero, the evolution of θ_t shows different behavior. When the zero lies in the upper half-plane, the contributions to the transmission phase from the zero-pole pair add up leading to the change of 2π over the zero-pole pair. On the other hand, two contributions are canceled by each other leading to the net change of 0 in the transmission phase when the zero lies in the lower-half plane.

III. AB RING WITH AN EMBEDDED DOUBLE-BARRIER WELL

In this section we study the scattering matrix of the AB ring when the double-barrier well (shown in Fig. 4) is inserted in the lower arm.

The symmetric double-barrier well can be described by the scattering matrix S_0 whose elements are given by the equations,

$$r_0 = r'_0 = \frac{\sqrt{1-T_0}(1-e^{2iKa})}{1-(1-T_0)e^{2iKa}}, \quad (15a)$$

$$t_0 = t'_0 = \frac{-T_0e^{iKa}}{1-(1-T_0)e^{2iKa}}. \quad (15b)$$

Here $K = \sqrt{k_F^2 + 2meV_g/\hbar^2}$ is the wave number inside the double-barrier well, a is the distance between two barriers, and V_g is the gate voltage capacitively coupled to the double-barrier well. The position of the resonant energy levels in the double-barrier well is controlled by the gate voltage V_g . The incident electrons are confined to the Fermi level with the Fermi wave number k_F . Two barriers are assumed to be identical and to be described by the scattering matrix,

$$S_b = \begin{pmatrix} \sqrt{1-T_0} & -i\sqrt{T_0} \\ -i\sqrt{T_0} & \sqrt{1-T_0} \end{pmatrix}, \quad (16)$$

where T_0 is the tunneling probability through the barrier. The transmission poles of t_0 (double-barrier well) are easily identified as

$$K_p a = n\pi - i\Gamma, \quad \Gamma \equiv \frac{1}{2} \log \frac{1}{1-T_0}, \quad (17)$$

where n is a positive integer. If the barriers' scattering matrix is of the form given by the Eq. (20), the poles are shifted by $\pi/2$. We note that t_0 can be expressed as the sum of simple poles,

$$t_0 = -\frac{i}{2}T_0e^{iKa} \sum_n \frac{1}{Ka - n\pi + i\Gamma}. \quad (18)$$

The transmission probability $|t_0|^2$ consists of a series of evenly spaced peaks with the same linewidth Γ . Transmission zeros are absent in the double-barrier resonant tunneling system.

We now study the properties of the transmission amplitude for the AB ring with an embedded double-barrier well. Inserting the scattering matrix S_0 of the double-barrier well into the general expression of the S -matrix of the AB ring (Appendix A), we compute the transmission amplitude numerically. The results are displayed in Fig. 5. In the numerical works, we use the model parameters: $k_FL = 5\pi/3(2\pi \text{ mod.})$; $\epsilon = 1/2$, $\lambda_1 = \lambda_2 = 1$ for the identical three-way splitters at the right and left junctions; $T_0 = 0.2$ for the transmission probability of the double-barrier well. One closed orbit in the complex t plot is completed with the variation of $\Delta(Ka) = 2\pi$. In the double-barrier well⁹, the orbit of t is closed with the period 2π of Ka . Comparing our results to the Fig. 1 in the work⁹ of Taniguchi and Büttiker, the orbit of t for the AB ring is featured with an additional closed lobe. This lobe passes through the origin when $\phi = 0$ or π . But note that the lobe disappears in t for some range

of ϕ . See the dotted line($\phi = 135^\circ$) in Fig. 5(a) and the long dashed line($\phi = 315^\circ$) in Fig. 5(d).

When $\phi = 0$ or π , the trajectory of t passes through the origin twice to complete the closed orbit. The transmission phase θ_t jumps by π at the transmission zeros [see the solid line in Fig. 5 (b) and the dot-dashed line in Fig. 5 (e)] since the transmission zeros are real. The phase increases by π at one zero and decreases by π at the other zero. These two real zeros are typical and behave differently when $\phi \neq 0$ or π , as will be shown later. Each transmission pole of the double-barrier well is paired with one transmission zero in the AB ring. The transmission zeros in the AB ring is the consequence of the destructive interference between two arms. As shown in Fig. 5(c) and (f), the zero-pole pairs are developed in the order: zero-zero-pole-pole.

When $\phi \neq 0$ or π , all the trajectories of t encircle the origin. These orbits can be considered as the combination of the two orbits: one(class III) encircles the origin while the other(class II) does not. Comparing $|t|^2$ and θ_t between Figs. 3 and 5, we can deduce that the transmission zeros are shifted off the real-energy axis. This point will be discussed later.

Let us study the structure of the poles and the zeros in detail. We focus on the two consecutive zero-pole pairs: one near $Ka = 2\pi$ and the other near $Ka = 3\pi$. These two zeros are typical in the sense that the others are the exact copy of these two in the physical properties. The nature of these two zeros is different since they behave in the opposite way under the magnetic fields (see Fig. 6.) When $\phi = 0$, we can deduce from Fig. 5 (b) and (c) that the zero-pole pairs are ordered in the sequence: pole-zero-zero-pole. When $0 < \phi < \pi$, we conclude, using the results of the Sec. II, for the zero-pole pair near $Ka = 2\pi$ that the zero(pole) lies in the upper(lower) half-plane of the complex-energy plane, respectively. On the other hand, the zero-pole pair near $Ka = 3\pi$ is in the lower half-plane. This is the reason why the phase change is 2π over the first zero-pole pair and is 0 over the second zero-pole pair. When $\phi = \pi$, the zero-pole pairs appear in the sequence: zero-pole-pole-zero. When $\pi < \phi < 2\pi$, the roles of two afore-mentioned zero-pole pairs are interchanged compared to the case of $0 < \phi < \pi$.

We compute the traces of the transmission zeros $Z_z(\phi)$ in the complex-energy plane ($z = Ka$) as a function of the magnetic AB phase ϕ .

$$Z_z(\phi) = E_z + \zeta(\phi). \quad (19)$$

Here E_z is the transmission zero when $\phi = 0$ and $\zeta(\phi)$ is the shift of the zero in the presence of the magnetic AB flux. There are two distinct zeros in the AB ring with the double-barrier well and the behavior of two zeros is different under the magnetic AB flux. The real and imaginary parts of $\zeta(\phi)$ are plotted in Fig. 6 for two zeros of $E_z = Ka = 2\pi$ [panel (a)] and of $E_z = Ka \approx 2.8775 \times \pi$ [panel (b)]. The real part of the first(second) zero is shifted downward(upward) under the magnetic fields, respectively. The minimum in $T = |t|^2$ [see Fig. 5 (c) and

(e)] shows this trend. The two zeros show the opposite behavior in their imaginary parts under the magnetic fields, too. The zero $E_z = 2\pi(2.8775 \times \pi)$ lies in the upper(lower) half-plane when $0 < \phi < \pi$, and in the lower(upper) half-plane when $\pi < \phi < 2\pi$, respectively. This corroborates our conclusion in the previous paragraph. Two zeros are on the real-energy axis when $\phi = n\pi$ with n being an integer.

To summarize, there are two types of the transmission zeros which can be distinguished in their behavior under magnetic fields. Since one pole is always paired with one zero, the change in the transmission phase over the zero-pole pair is 0 or 2π depending on the position of the zero in the complex-energy plane.

IV. AB INTERFEROMETER WITH AN EMBEDDED T -STUB

In this section, we consider the AB ring with the side-branch or the t -stub. The t -stub provides the different type of resonant levels compared to the double-barrier well. In contrast to the double-barrier well, the t -stub itself provides the transmission zeros as well as the transmission poles. In this work, we consider the t -stub structure with two tunneling barriers which was previously studied in the literature^{11,12}. We use the most symmetric three-way splitter at the junction with the parameters¹², $\epsilon = 4/9$, $\lambda_1 = -1$ and $\lambda_2 = 1$. The double-barrier is assumed not to provide any resonant energy levels or the distance between two barriers is so short that the energy level spacing is much larger than any other interesting energy scale in the problem. The introduction of two additional barriers to the t -stub enables us to control the tunneling strength through the t -stub structure and to mimic the quantum dot system. The S -matrix of the two barriers is chosen to be

$$S_b = \begin{pmatrix} i\sqrt{1-T_0} & \sqrt{T_0} \\ \sqrt{T_0} & i\sqrt{1-T_0} \end{pmatrix}, \quad (20)$$

where T_0 is the tunneling probability through the barrier. We have chosen the different overall phase for S_b compared to the double-barrier well. The S -matrix of the t -stub with the double barriers is formulated in the Appendix B.

To get some insights on the position of the transmission zeros and poles, we consider the S -matrix of the simple t -stub. The incoming and outgoing current amplitudes can be matched at the junction of the t -stub.

$$\begin{pmatrix} O_S \\ O_L \\ O_R \end{pmatrix} = \begin{pmatrix} \sigma_t & \sqrt{\epsilon_t} & \sqrt{\epsilon_t} \\ \sqrt{\epsilon_t} & a_t & b_t \\ \sqrt{\epsilon_t} & b_t & a_t \end{pmatrix} \begin{pmatrix} I_S \\ I_L \\ I_R \end{pmatrix}. \quad (21)$$

Here I 's and O 's are the incoming and outgoing current amplitudes at the junction. $\sigma_t = -a_t - b_t$ and a_t, b_t can be determined to satisfy the unitarity of the scattering

matrix.

$$a_t = \frac{1}{2} [\lambda_1 + \lambda_2 \sqrt{1-2\epsilon_t}], \quad (22a)$$

$$b_t = \frac{1}{2} [-\lambda_1 + \lambda_2 \sqrt{1-2\epsilon_t}]. \quad (22b)$$

There are four possible choices with $\lambda_i = \pm 1 (i = 1, 2)$. The value of ϵ_t is constrained: $0 \leq \epsilon_t \leq 1/2$. When there is an infinite potential wall at the end of the stub of length a , O_S and I_S are related to each other by $I_S = O_S e^{i(2Ka+\pi)}$. The additional phase π guarantees the node of the wave function at the infinite wall. The wave number K in the stub is given by $K = \sqrt{k_F^2 + 2meV_g/\hbar^2}$. The quasibound state energy levels in the stub can be shifted with the gate voltage V_g (capacitively coupled to the t -stub). The effective S -matrix can be readily derived

$$\begin{pmatrix} O_L \\ O_R \end{pmatrix} = S_0 \begin{pmatrix} I_L \\ I_R \end{pmatrix}, \quad S_0 = \begin{pmatrix} r_0 & t_0 \\ t_0 & r_0 \end{pmatrix}, \quad (23a)$$

$$t_0 = b_t - \frac{\epsilon_t z}{1 + \sigma z} = \frac{b_t(1 + \lambda_1 z)}{1 - (a_t + b_t)z}, \quad (23b)$$

$$r_0 = a_t - \frac{\epsilon z}{1 + \sigma z} = \frac{a_t(1 - \lambda_1 z)}{1 - (a_t + b_t)z}. \quad (23c)$$

Here $z = e^{2iKa}$. The first terms in t_0 and r_0 represent the direct scattering process and the second term comes from the multiple scattering processes in the stub. The unitarity of S can be proved by showing that

$$|r|^2 + |t|^2 = 1, \quad t^* r + r^* t = 0 \quad (24)$$

The transmission poles and zeros are located at

$$Z_z = \left(n + \frac{1 + \lambda_1}{4}\right) \pi, \quad (25a)$$

$$Z_p = \left(n + \frac{1 - \lambda_2}{4}\right) \pi - \frac{i}{2} \log \frac{1}{\sqrt{1-2\epsilon_t}}, \quad (25b)$$

respectively. Here n is an integer. For our choice of $\lambda_1 = -1$ and $\lambda_2 = 1$ for the t -stub, $Z_z = n\pi$ and $\text{Re}Z_p = n\pi$.

The scattering matrix of the t -stub with the double-barrier is derived in the Appendix B. Note that addition of the two barriers to the t -stub does not change the transmission zeros, but the poles are modulated by T_0 in both the real and the imaginary parts.

The transmission amplitudes of the whole AB ring are computed numerically using the formulation detailed in the Appendix A and B and are presented in Fig. 8. The model parameters are: $\epsilon = 1/2$, $\lambda_1 = -1$, and $\lambda_2 = 1$ for the Shapiro matrices at the left and right three-way junctions. The three-way splitter for the t -stub was chosen to be the most symmetric one as noted above. The tunneling barriers for the t -stub are chosen as $T_0 = 0.8$.

As can be deduced from the Fig. 8 (c) and (f), the zero-pole pairs appear in the order: zero-pole-zero-pole. All the trajectories of t are circles and the closed orbit is completed with $\Delta Ka = \pi$. Three different classes of

orbits of t are realized for this system with varying the magnetic AB flux.

When $\phi = 0$ or $\phi = \pi$, the transmission zero lies on the real-energy axis and the transmission phase jumps by π at the zeros. When $\phi = 0$, θ_t near $Ka = 2\pi$ drops by π at the zero and increases smoothly by the amount π due to the pole. For this zero-pole pair, the zero precedes the pole as shown in Fig. 8 (b) and (c). When $\phi = \pi$, θ_t drops by π at the zero and increases almost linearly due to the pole. We can deduce from the functional shape of the θ_t and $T = |t|^2$ [see Fig. 8 (e) and (f)] that the zeros and poles are almost evenly interlaced.

When $0 < \phi < \pi$, the orbits of t encircle the origin and the phase evolution of θ_t is smooth and continuous. The orbits move away from the origin with increasing the AB phase. This trend is clearly visible in Fig 8 (a) and (c). Since the zeros lie in the upper half-plane and the poles are in the lower half-plane, two contributions add up and leading to the change by 2π over the zero-pole pair.

The orbits of t lie outside the origin when $\pi < \phi < 2\pi$. In this case, the zeros and the poles lie in the same lower half-plane. Their contributions to the transmission phase cancel each other, leading to the net change of θ_t over the zero-pole pair is zero. Since the phase decreasing precedes the phase increasing, the zeros precedes the poles. The zero-pole pair is closing to each other as the value of ϕ is increased from π to 2π .

The traces of the transmission zeros $Z_z(\phi)$ in the complex-energy plane ($z = Ka$) are computed and plotted in Fig. 9 as a function of the magnetic AB phase ϕ .

$$Z_z(\phi) = E_z + \zeta(\phi). \quad (26)$$

Here E_z is the transmission zero when $\phi = 0$ and $\zeta(\phi)$ is the shift of the zero in the presence of the magnetic AB flux. In contrast to the AB ring with the double-barrier well, the nature of all zeros is identical in the sense that their behavior is the same under the magnetic fields. The real and imaginary parts of $\zeta(\phi)$ are plotted in Fig. 9 for the zero of $E_z = Ka \approx 1.9565 \times \pi$. Note that this zero in the AB ring is shifted from $E_z = 2\pi$ of the t -stub with the double-barrier. As expected from the shift of the minimum position of $T = |t|^2$ [see Fig. 8 (c) and (e)], the real part of the zero is positively shifted in the presence of the magnetic fields. The imaginary part of the zero is sinusoidal as a function of the AB phase ϕ and vanishes when the magnetic AB flux is an integer or a half-integer multiple of the flux quantum.

V. SUMMARY AND CONCLUSION

In this paper, we studied the behavior of the transmission zeros and the corresponding changes in the transmission phase when the time-reversal symmetry of the system is broken by magnetic fields. For our study we considered the Aharonov-Bohm(AB) interferometers with one scattering center in the lower arm. Studied

scattering centers include the system of one discrete energy level, the double-barrier well, and the t -stub with the double barriers. Each resonant level in the scattering center gives rise to a transmission pole and is paired with a transmission zero in the AB ring. Due to the causality relation, the transmission pole always lies in the lower half-plane of the complex-energy plane. On the other hand, the zero can be anywhere in the complex-energy plane and its position can be controlled by the magnetic AB flux. Depending on the position of the transmission zeros in the complex-energy plane, the trajectory and the phase of the transmission amplitude show different behaviors.

The transmission zeros lie on the real-energy axis when the magnetic AB flux is an integer or a half-integer multiple of the flux quantum. The transmission phase jumps by π at the transmission zeros in this case.

The transmission zeros are shifted off the real-energy axis and can be either in the upper or in the lower half-plane of the complex-energy plane, when the AB magnetic flux is off the integer or a half-integer multiple of the flux quantum. The evolution of the transmission phase in this case is continuous as the Fermi level is scanned through the real part of the transmission zeros.

When the zeros lie in the lower half-plane, the orbits of the transmission amplitude lie outside the origin and the phase change is limited by the two extreme points of the orbit when viewed from the origin. Since the zero-pole pair contributes the opposite sign of the phase by π , the net change in the transmission phase over the zero-pole pair is zero.

The orbits of the transmission amplitude encircle the origin when the zeros lie in the upper-half plane. In this case, the zero-pole pair give the same sign of the phase by π to the transmission phase, the total accrued phase over this zero-pole pair is 2π .

Though the zero-pole pair leads to the different phase evolution depending on the position of the zero in the complex-energy plane, the transmission phase remains in phase after passing through the zero-pole pair.

The modulation of the transmission zeros in the closed AB ring may be tested in experiments using the following setup. We may insert the closed AB ring into one arm of the larger AB ring. The larger AB ring should be the open system where the multiple windings of the electrons are prevented. The evolution of the transmission phase in the closed AB ring can be measured by making the period of the AB oscillation in the larger ring much shorter than that of the closed AB ring.

Acknowledgments

We are indebted to H. W. Lee for useful discussions. This work was supported in part by the BK21 project and in part by grant No. 1999-2-114-005-5 from the KOSEF.

APPENDIX A: *S*-MATRIX OF AHARONOV-BOHM RING

In this Appendix, we want to derive in a compact form the *S*-matrix of an AB ring when some scattering centers are present on the AB ring, especially when the interesting target system is inserted in the lower arm of the AB ring as shown in Fig. 1. The amplitudes of the incoming and outgoing waves at the left and right junctions are related to each other by the scattering matrix.

$$\begin{pmatrix} O_L \\ x_1 \\ x_2 \end{pmatrix} = S^L \begin{pmatrix} I_L \\ y_1 \\ y_2 \end{pmatrix}, \quad \begin{pmatrix} O_R \\ v_1 \\ v_2 \end{pmatrix} = S^R \begin{pmatrix} I_R \\ u_1 \\ u_2 \end{pmatrix}, \quad (\text{A1a})$$

$$S^p = \begin{pmatrix} \sigma_p & \sqrt{\epsilon_p} & \sqrt{\epsilon_p} \\ \sqrt{\epsilon_p} & a_p & b_p \\ \sqrt{\epsilon_p} & b_p & a_p \end{pmatrix}, \quad p = L, R. \quad (\text{A1b})$$

Here $S^{L,R}$ are the Shapiro matrices responsible for the splitting of the electron wavefunctions in three pathways. The unitarity leads to four possible solutions,

$$\sigma_p = -a_p - b_p, \quad (\text{A2a})$$

$$a_p = \frac{1}{2} [\lambda_1^p + \lambda_2^p \sqrt{1 - 2\epsilon_p}], \quad (\text{A2b})$$

$$b_p = \frac{1}{2} [-\lambda_1^p + \lambda_2^p \sqrt{1 - 2\epsilon_p}], \quad (\text{A2c})$$

where $\lambda_1^p, \lambda_2^p = \pm 1$. To simplify the algebra, we introduce new notations,

$$S_p \equiv \begin{pmatrix} a_p & b_p \\ b_p & a_p \end{pmatrix}, \quad |s_p\rangle \equiv \begin{pmatrix} \sqrt{\epsilon_p} \\ \sqrt{\epsilon_p} \end{pmatrix}. \quad (\text{A3})$$

$S_{L,R}$ is the 2×2 submatrix of $S^{L,R}$, respectively. The amplitudes of waves at the left and right junctions are related to each other by the scattering matrix which is responsible for the scattering processes in the two arms,

$$\begin{pmatrix} |y\rangle \\ |u\rangle \end{pmatrix} = \begin{pmatrix} \mathcal{R} & \mathcal{T}' \\ \mathcal{T} & \mathcal{R}' \end{pmatrix} \begin{pmatrix} |x\rangle \\ |v\rangle \end{pmatrix}. \quad (\text{A4})$$

The ket vectors are defined, e.g., as $|x\rangle \equiv \begin{pmatrix} x_1 \\ x_2 \end{pmatrix}$. \mathcal{R} and \mathcal{T} are the 2×2 matrices which contain the information of the scattering matrices in each arm and the phase accrued by the motion of electrons along the ring. These matrices are model-specific and are discussed in the main text. We want to find the *S*-matrix of the ring.

$$O_L = \sigma_L I_L + \langle s_L | y \rangle, \quad (\text{A5a})$$

$$O_R = \sigma_R I_R + \langle s_R | u \rangle, \quad (\text{A5b})$$

$$|x\rangle = I_L |s_L\rangle + S_L |y\rangle, \quad (\text{A5c})$$

$$|v\rangle = I_R |s_R\rangle + S_R |u\rangle. \quad (\text{A5d})$$

From the above equations, it is straightforward to derive the following results,

$$|y\rangle = I_L \cdot [1 - \overline{\mathcal{R}} S_L]^{-1} \overline{\mathcal{R}} |s_L\rangle + I_R \cdot [1 - \overline{\mathcal{R}} S_L]^{-1} \overline{\mathcal{T}}' |s_R\rangle, \quad (\text{A6a})$$

$$|u\rangle = I_L \cdot [1 - \overline{\mathcal{R}}' S_R]^{-1} \overline{\mathcal{T}} |s_L\rangle + I_R \cdot [1 - \overline{\mathcal{R}}' S_R]^{-1} \overline{\mathcal{R}}' |s_R\rangle, \quad (\text{A6b})$$

where newly defined reflection and transmission matrices are given by the expressions,

$$\overline{\mathcal{R}} = \mathcal{R} + \mathcal{T}' [1 - S_R \mathcal{R}']^{-1} S_R \mathcal{T}, \quad (\text{A7a})$$

$$\overline{\mathcal{T}} = \mathcal{T} [1 - S_L \mathcal{R}]^{-1}, \quad (\text{A7b})$$

$$\overline{\mathcal{R}}' = \mathcal{R}' + \mathcal{T} [1 - S_L \mathcal{R}]^{-1} S_L \mathcal{T}', \quad (\text{A7c})$$

$$\overline{\mathcal{T}}' = \mathcal{T}' [1 - S_R \mathcal{R}']^{-1}. \quad (\text{A7d})$$

After more algebra, we find the *S*-matrix of the ring,

$$\begin{pmatrix} O_L \\ O_R \end{pmatrix} = S_{\text{ring}} \begin{pmatrix} I_L \\ I_R \end{pmatrix}, \quad (\text{A8a})$$

$$S_{\text{ring}} = \begin{pmatrix} r_{LL} & t_{LR} \\ t_{RL} & r_{RR} \end{pmatrix}, \quad (\text{A8b})$$

$$r_{LL} = \sigma_L + \langle s_L | [1 - \overline{\mathcal{R}} S_L]^{-1} \overline{\mathcal{R}} | s_L \rangle, \quad (\text{A8c})$$

$$r_{RR} = \sigma_R + \langle s_R | [1 - \overline{\mathcal{R}}' S_R]^{-1} \overline{\mathcal{R}}' | s_R \rangle, \quad (\text{A8d})$$

$$t_{LR} = \langle s_L | [1 - \overline{\mathcal{R}} S_L]^{-1} \overline{\mathcal{T}}' | s_R \rangle, \quad (\text{A8e})$$

$$t_{RL} = \langle s_R | [1 - \overline{\mathcal{R}}' S_R]^{-1} \overline{\mathcal{T}} | s_L \rangle. \quad (\text{A8f})$$

APPENDIX B: SCATTERING MATRIX OF THE *t*-STUB WITH DOUBLE BARRIERS

We consider the *S*-matrix of the *t*-stub with the double barriers [see Fig. 7]. The distance between two barriers is assumed to be too short to allow the resonant energy levels or the energy level spacing is very large compared to other energy scales. But the length of the stub, *a*, is long enough to allow the quantized energy levels in the isolated stub. In this case, the amplitude of the wavefunctions can be matched as

$$\begin{pmatrix} O_s \\ x_1 \\ x_2 \end{pmatrix} = S^t \begin{pmatrix} I_s \\ y_1 \\ y_2 \end{pmatrix}, \quad S^t = \begin{pmatrix} \sigma & \sqrt{\epsilon} & \sqrt{\epsilon} \\ \sqrt{\epsilon} & a & b \\ \sqrt{\epsilon} & b & a \end{pmatrix} \quad (\text{B1a})$$

$$\begin{pmatrix} O_L \\ y_1 \end{pmatrix} = S_L \begin{pmatrix} I_L \\ x_1 \end{pmatrix}, \quad \begin{pmatrix} O_R \\ y_2 \end{pmatrix} = S_R \begin{pmatrix} I_R \\ x_2 \end{pmatrix},$$

$$S_p = \begin{pmatrix} r_p & t'_p \\ t_p & r'_p \end{pmatrix}, \quad p = L, R. \quad (\text{B1b})$$

We want to find the *S*-matrix of the *t*-stub with the double barriers,

$$\begin{pmatrix} O_L \\ O_R \end{pmatrix} = S \begin{pmatrix} I_L \\ I_R \end{pmatrix}. \quad (\text{B2})$$

When there is an infinite potential wall at the end of the stub, two amplitudes I_s and O_s are constrained as $I_s = e^{i(2Ka+\pi)} O_s$. We can rewrite the above relations between the amplitudes as

$$O_s = \sigma I_s + \langle s_t | y \rangle, \quad (\text{B3a})$$

$$|x\rangle = I_s |s_t\rangle + S_t |y\rangle, \quad (\text{B3b})$$

$$|O\rangle = R |I\rangle + T' |x\rangle, \quad (\text{B3c})$$

$$|y\rangle = T |I\rangle + R' |x\rangle. \quad (\text{B3d})$$

New notations are introduced to simplify the algebra.

$$|x\rangle = \begin{pmatrix} x_1 \\ x_2 \end{pmatrix}, \quad |y\rangle = \begin{pmatrix} y_1 \\ y_2 \end{pmatrix}, \quad (\text{B4a})$$

$$|I\rangle = \begin{pmatrix} I_L \\ I_R \end{pmatrix}, \quad |O\rangle = \begin{pmatrix} O_L \\ O_R \end{pmatrix}, \quad (\text{B4b})$$

$$|s_t\rangle = \begin{pmatrix} \sqrt{\epsilon} \\ \sqrt{\epsilon} \end{pmatrix}, \quad S_t = \begin{pmatrix} a & b \\ b & a \end{pmatrix}, \quad (\text{B4c})$$

$$R = \begin{pmatrix} r_L & 0 \\ 0 & r_R \end{pmatrix}, \quad T = \begin{pmatrix} t_L & 0 \\ 0 & t_R \end{pmatrix},$$

$$R' = \begin{pmatrix} r'_L & 0 \\ 0 & r'_R \end{pmatrix}, \quad T' = \begin{pmatrix} t'_L & 0 \\ 0 & t'_R \end{pmatrix}. \quad (\text{B4d})$$

From the relation between I_s and O_s , we find

$$\begin{aligned} I_s &= -\frac{1}{\sigma + e^{-2iKa}} \langle s_t | y \rangle \\ &= -\frac{\langle s_t | [1 - R'S_t]^{-1} T | I \rangle}{\sigma + e^{-2iKa} + \langle s_t | [1 - R'S_t]^{-1} R' | s_t \rangle}. \end{aligned} \quad (\text{B5})$$

After some algebra, we find the S -matrix of the system $|O\rangle = S_0 |I\rangle$,

$$\begin{aligned} S_0 &= R + T'[1 - S_t R']^{-1} S_t T \\ &\quad - \frac{T'[1 - S_t R']^{-1} |s_t\rangle \langle s_t| [1 - R'S_t]^{-1} T}{\sigma + e^{-2iKa} + \langle s_t | [1 - R'S_t]^{-1} R' | s_t \rangle}. \end{aligned} \quad (\text{B6})$$

Note that the transmission poles are determined by the zeros of $\sigma + e^{-2iKa} + \langle s_t | [1 - R'S_t]^{-1} R' | s_t \rangle$.

For the two identical barriers described by the scattering matrix ($R_0 = 1 - T_0$),

$$S_b = \begin{pmatrix} i\sqrt{R_0} & \sqrt{T_0} \\ \sqrt{T_0} & i\sqrt{R_0} \end{pmatrix}, \quad (\text{B7})$$

the scattering matrix of the t stub with double-barrier is given by the equations,

$$S_0 = \begin{pmatrix} r_0 & t_0 \\ t_0 & r_0 \end{pmatrix}, \quad (\text{B8a})$$

$$t_0 = \frac{T_0 b}{(1 - i\sqrt{R_0}a)^2 + R_0 b^2} \frac{e^{-2iKa} + \lambda_1}{e^{-2iKa} + \frac{\sigma + i\sqrt{R_0}}{1 + i\sqrt{R_0}\sigma}} \quad (\text{B8b})$$

$$\begin{aligned} r_0 &= i\sqrt{R_0} + \frac{T_0}{1 + i\sqrt{R_0}\sigma} \cdot \left[\frac{a + i\sqrt{R_0}(b^2 - a^2)}{1 - i\sqrt{R_0}(a - b)} \right. \\ &\quad \left. - \frac{\epsilon}{(1 + i\sqrt{R_0}\sigma)e^{-2iKa} + \sigma + i\sqrt{R_0}} \right]. \end{aligned} \quad (\text{B8c})$$

Note that the transmission zeros do not depend on or are not modified by the barriers' tunneling strength T_0 [see Eqs. (23b) and (25a)], but the poles are modulated by the value of T_0 . The transmission poles (Z_p) and zeros (Z_z) are located at

$$Z_z = \left(n + \frac{1 + \lambda_1}{4} \right) \pi, \quad (\text{B9a})$$

$$\begin{aligned} Z_p &= \left(n + \frac{1 - \lambda_2}{4} \right) \pi \\ &\quad + \frac{\lambda_2}{2} \left[\tan^{-1} \sqrt{\frac{R_0}{1 - 2\epsilon}} - \tan^{-1} \sqrt{R_0(1 - 2\epsilon)} \right] \\ &\quad - \frac{i}{2} \log \sqrt{\frac{1 + R_0(1 - 2\epsilon)}{1 - 2\epsilon + R_0}}. \end{aligned} \quad (\text{B9b})$$

As expected, the linewidth of quasibound states in the stub (or the imaginary part of poles) is reduced with the reduced T_0 .

¹ A. Yacoby, M. Heiblum, D. Mahalu, and H. Shtrikman, Phys. Rev. Lett. **74**, 4047 (1995).

² R. Schuster, E. Buks, M. Heiblum, D. Mahalu, V. Umansky, and H. Shtrikman, Nature **385**, 417 (1997).

³ E. Buks, R. Schuster, M. Heiblum, D. Mahalu, V. Umansky, and H. Shtrikman, Phys. Rev. Lett. **77**, 4664 (1996).

⁴ W. G. van der Wiel, S. De Franceschi, T. Fujisawa, J. M. Elzerman, S. Tarycha, and L. P. Kouwenhoven, Science **289**, 2105 (2000).

⁵ Y. Ji, M. Heiblum, D. Sprinzak, D. Mahalu, and H. Shtrikman, Science **290**, 779 (2000).

⁶ M. Büttiker, Phys. Rev. Lett. **57**, 1761 (1986).

⁷ D. C. Langreth, Phys. Rev. **150**, 516 (1966).

⁸ H. -W. Lee, Phys. Rev. Lett. **82**, 2358 (1999).

⁹ T. Taniguchi and M. Büttiker, Phys. Rev. B **60**, 13814 (1999).

¹⁰ H. -W. Lee, J. Korean Phys. Soc. **34**, S180 (1999).

¹¹ C. M. Ryu and S. Y. Cho, Phys. Rev. B **58**, 3572 (1998).

¹² Z. Shao, W. Porod, and C. S. Lent, Phys. Rev. B **49**, 7453 (1994).

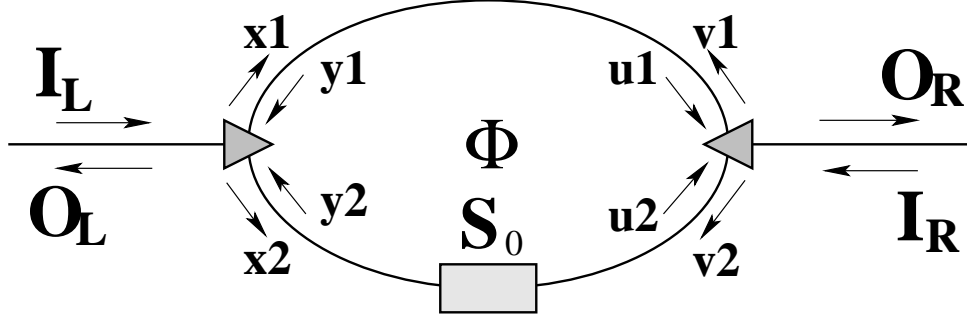


FIG. 1: Aharonov-Bohm ring with an embedded target system. The scattering process in the target system is described by the scattering matrix S_0 . The length of the upper and lower arms is denoted by L . Φ is the magnetic Aharonov-Bohm(AB) flux threading through the AB ring.

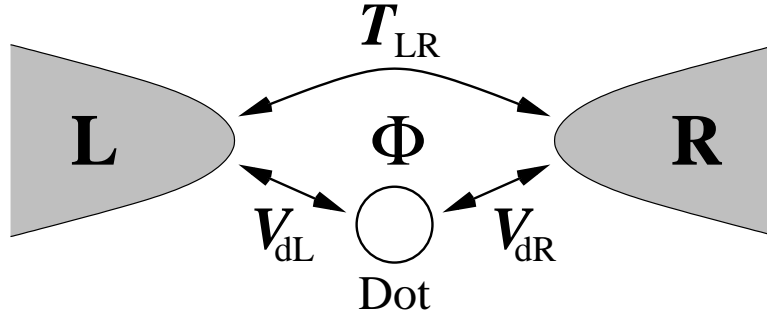


FIG. 2: Schematic display of Aharonov-Bohm(AB) interferometer with a quantum dot. The dot is modeled by one discrete energy level.

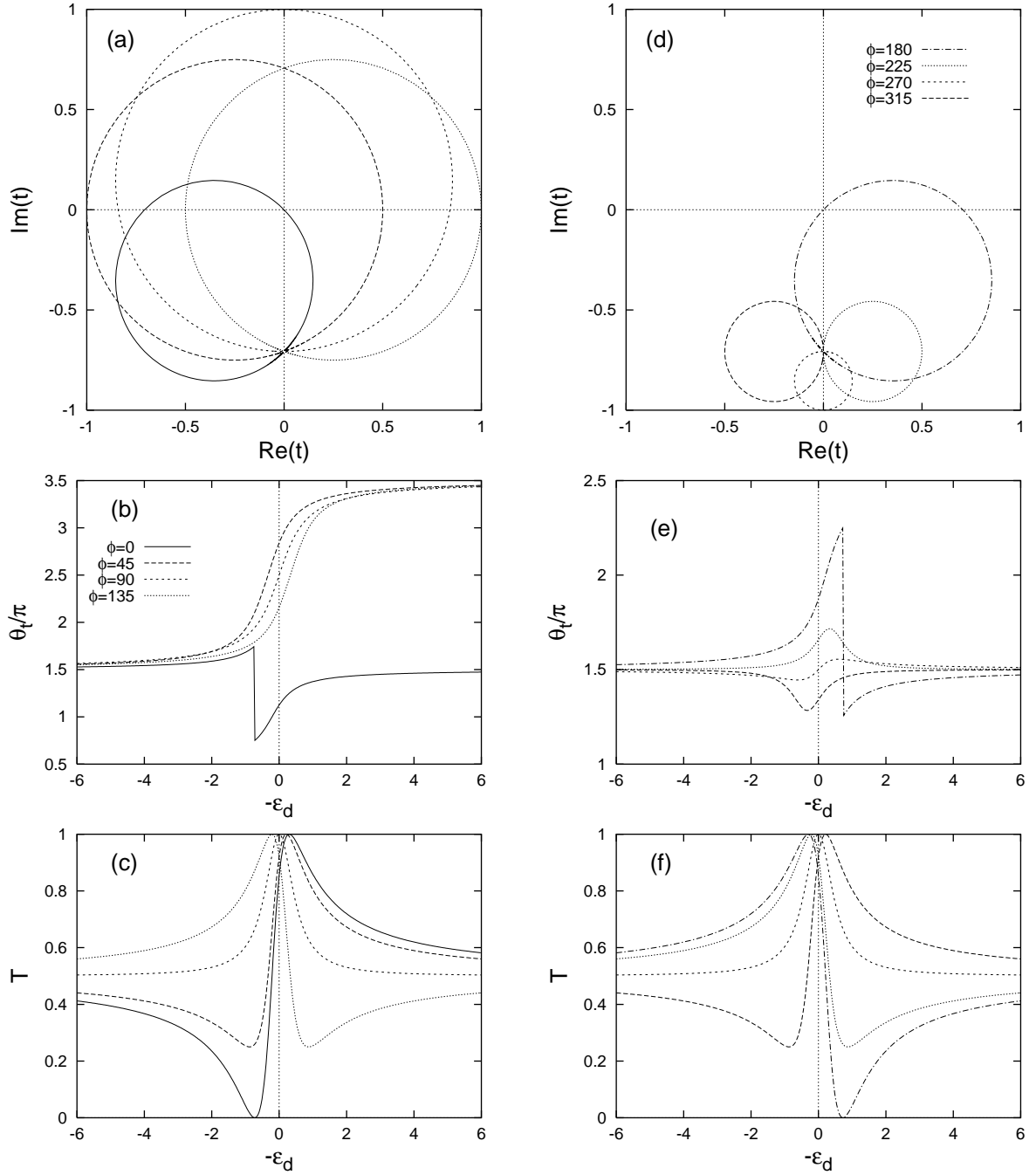


FIG. 3: Behavior of the transmission amplitude t with varying the AB phase ϕ for the AB interferometer with one discrete energy level. Panels (a) and (d) display the trajectories of t as an implicit function of the discrete energy level ϵ_d . The evolution of the transmission phase θ_t is shown in panels (b) and (e). The transmission probability $T = |t|^2$ is displayed in two panels (c) and (f). The AB phases are the same for the same lines either in the left column panels (a), (b) and (c) or in the right column panels (d), (e) and (f).

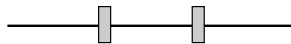


FIG. 4: Double-barrier well.

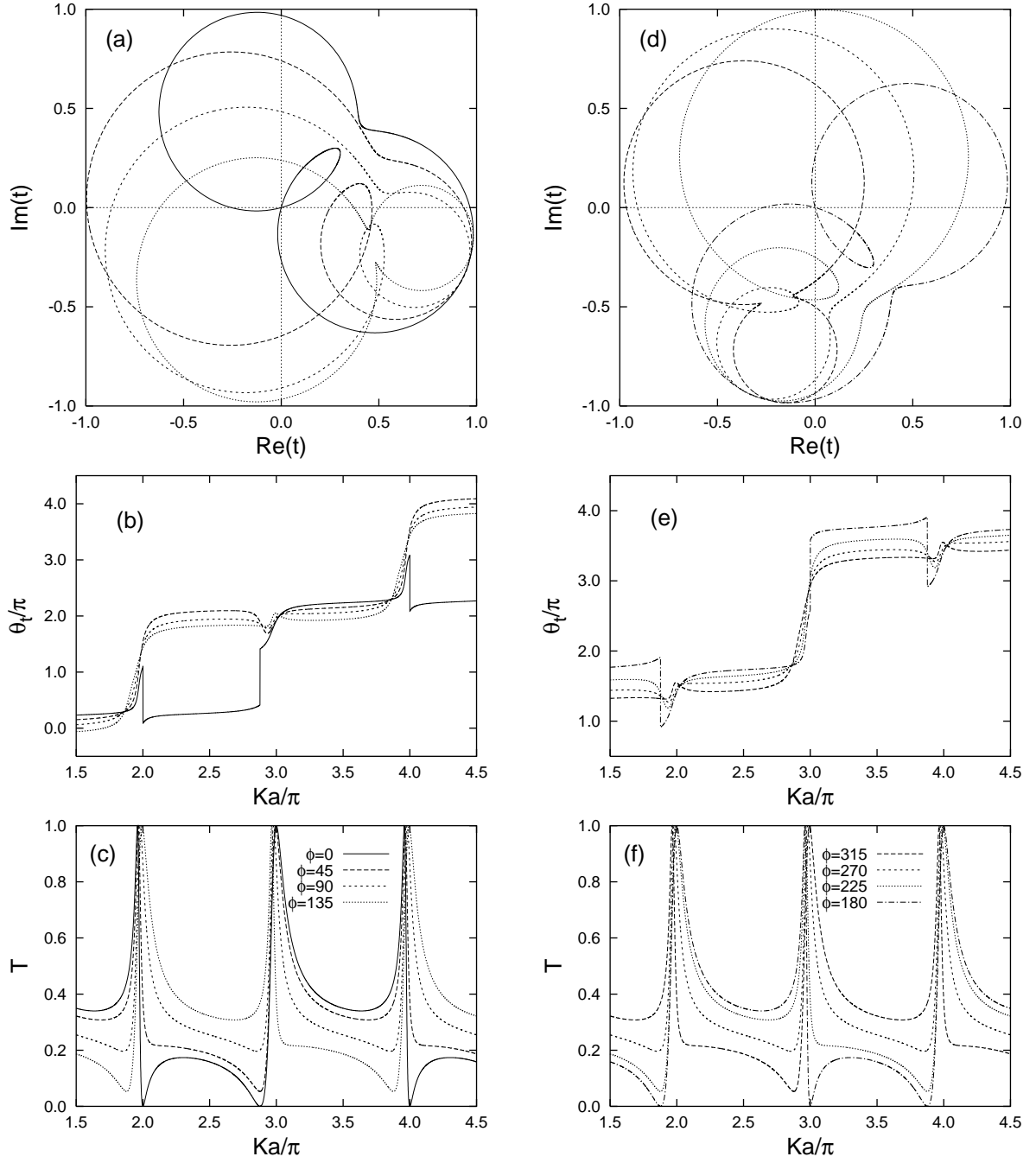


FIG. 5: Behavior of the transmission amplitude t with varying the AB phase ϕ for the AB ring with the double-barrier well. Panel descriptions are the same as in Fig. 3. Model parameters are chosen as $k_F L = 5\pi/3(\text{mod. } 2\pi)$, $\epsilon_{L,R} = 1/2$, $\lambda_1 = \lambda_2 = 1$ and $T_0 = 0.2$.

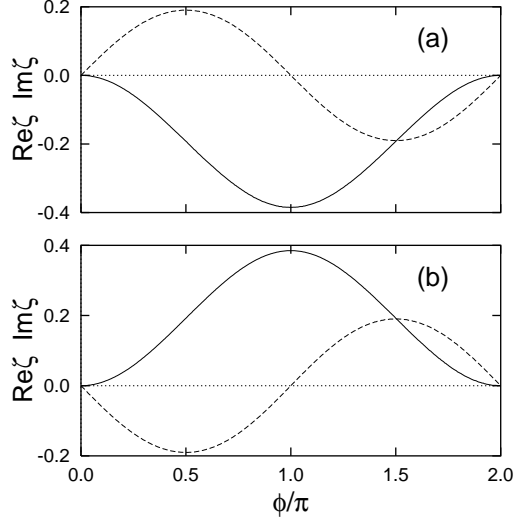


FIG. 6: Transmission zeros as a function of the AB phase ϕ in the AB ring with the double-barrier well. The AB phase dependence of the zero at $Ka = 2\pi[2.8775 \times \pi]$ is displayed in the panel (a)[(b)], respectively. Solid(dashed) line is the real(imaginary) part of the shifted zero $\zeta(\phi)$, respectively. The transmission zero is represented by $Z_z(\phi) = E_z + \zeta(\phi)$ where E_z is the transmission zero when $\phi = 0$ and $\zeta(\phi)$ is the shift of the zero in the presence of the magnetic AB flux.

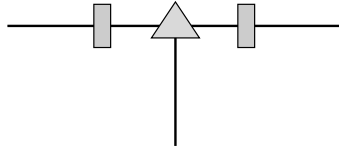


FIG. 7: t -stub with the double-barrier.

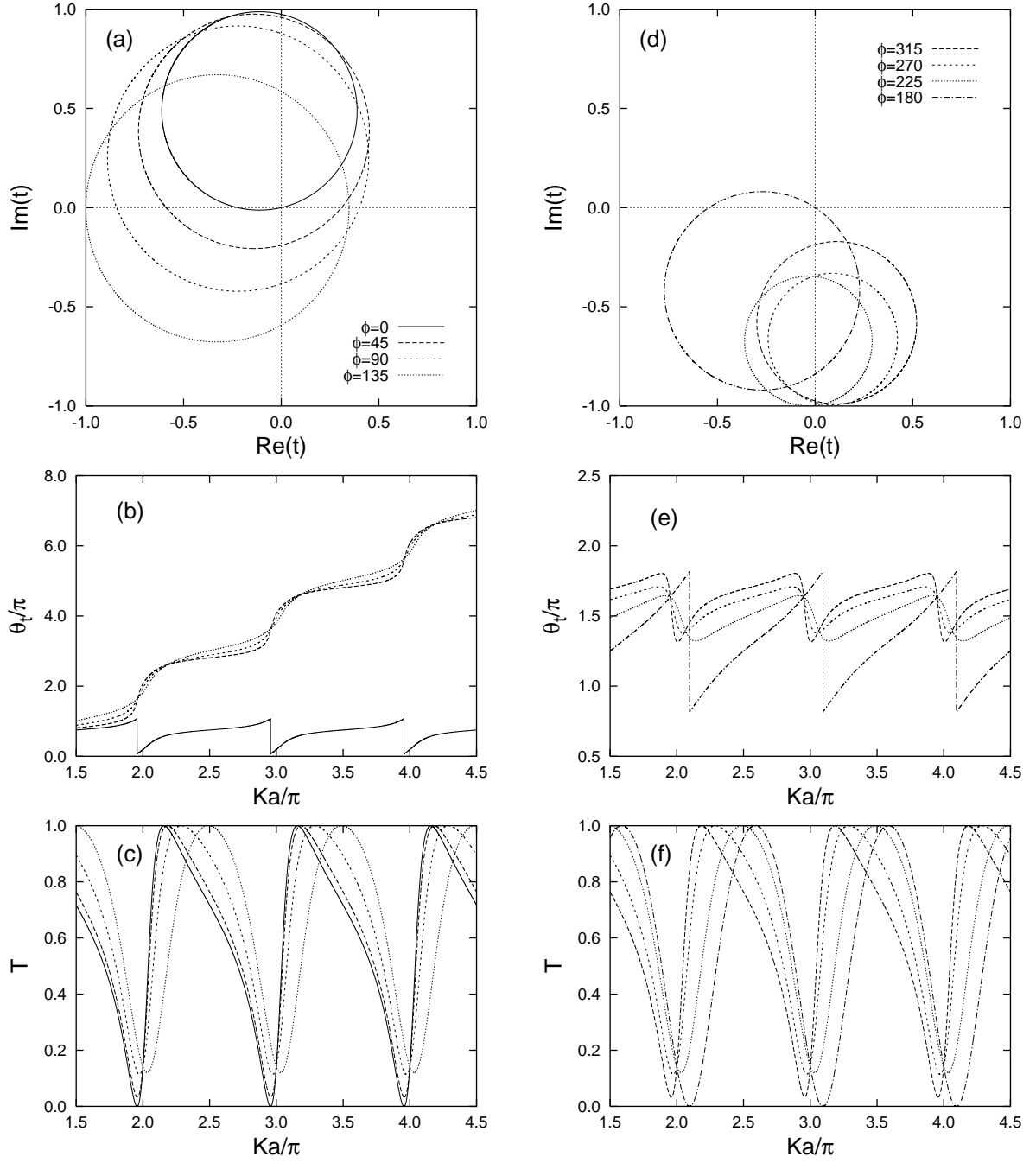


FIG. 8: Behavior of the transmission amplitude t with varying the AB phase ϕ for the AB ring with the t -stub. Panel descriptions are the same as in Fig. 3. Model parameters are chosen as $k_F L = \pi/2$; $\epsilon_{L,R} = 1/2$, $\lambda_{L,R1} = -1$, and $\lambda_{L,R2} = 1$; $\epsilon_t = 4/9$, $\lambda_{t1} = -1$ and $\lambda_{t2} = 1$; $T_L = T_R = 0.8$.

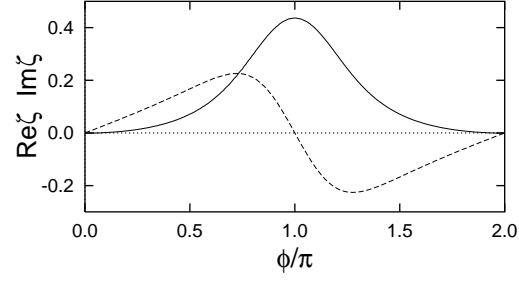


FIG. 9: Transmission zeros as a function of the AB phase ϕ in the AB ring with the t -stub system. Solid(dashed) line is the real(imaginary) part of the shifted zero $\zeta(\phi)$, respectively.